Supplemental Material for "Impact of long-term erosion on crustal stresses and seismicity in stable continental regions": Model setup, yield stress classes, lithosphere mechanical response, fault stability margin, and earthquake depths

This supplementary material provides information on (A) model setup and parameters (Table S1), (B) model differential stress characteristics and classes (Figure S2), and (C) model uplift and stress response to erosion (Figures S3-S8). Section (D) gives details of the Fault Stability Margin construction and evolution for Andersonian fault geometries (Figure S8). Section (E) gives information on large earthquake rupture depths (Table S2) and seismicity catalog in Figure 3b.

(A) MODEL SETUP

Models are constructed with two elasto-visco-brittle layers (crust and mantle). The brittle rheology is defined by the Drucker-Prager failure criterion:

$$J_2 = -\frac{1}{3}J_1 + \frac{C}{\tan\varphi}, \quad (1)$$

where J_1 and J_2 are the first and second invariants of the stress tensor, C is the material cohesion ($C = 10^7$ Pa), and φ is the internal friction angle ($\varphi = 15°$, equivalent to a Mohr-Coulomb friction angle of 30°). The ductile rheology is based on the power-law dislocation creep:

$$(\sigma_1 - \sigma_3) = \left(\frac{\dot{\varepsilon}}{A}\right)^{-n} exp\left(\frac{Q}{nRT}\right), \quad (2)$$

where σ_1 and σ_3 are the maximum and minimum principal stresses, $\dot{\varepsilon}$ is the scalar strain rate (s^{-1}), T is the temperature (K) and R is gas constant ($R = 8.31$ $J\ mol^{-1}\ K^{-1}$). A, Q and n are the dislocation creep parameters specific for a given material (Table S1).

Table S1. Model rheology parameters

			Elasticity		Brittle failure		Dislocation creep			
Material	**Layer**	**ρ (kg m^{-3})**	**E (Pa)**	**ν**	**C (Pa)**	**φ (°)**	**A (Pa^{-n} s^{-1})**	**Q (J mol^{-1})**	**n**	**Ref.**
quartz	crust	2800	1×10^{11}	0.3	1×10^{7}	15	3.9×10^{-34}	135×10^{3}	4	(1)
diabase	crust	2800	1×10^{11}	0.3	1×10^{7}	15	1.2×10^{-26}	485×10^{3}	4.7	(2)

olivine	mantle	3300	1×10^{11}	0.3	1×10^{7}	15	1.1×10^{-16}	530×10^{3}	3.5	(3)

Ref.: (1) (Luan and Paterson, 1992), (2) (Wilks and Carter, 1990), (3) (Hirth and Kohlstedt, 2003)

The models are subjected to a constant erosion rate (chosen between 4 and 200 m/m.y.) at their center (-50 ≤ x ≤ 50 km, Fig. 1). The erosion rate is kept constant during the whole experiment (10 m.y.), without dependency on surface elevation or topography.

(B) MODEL DIFFERENTIAL STRESS PROFILES AND STRENGTH CLASSES

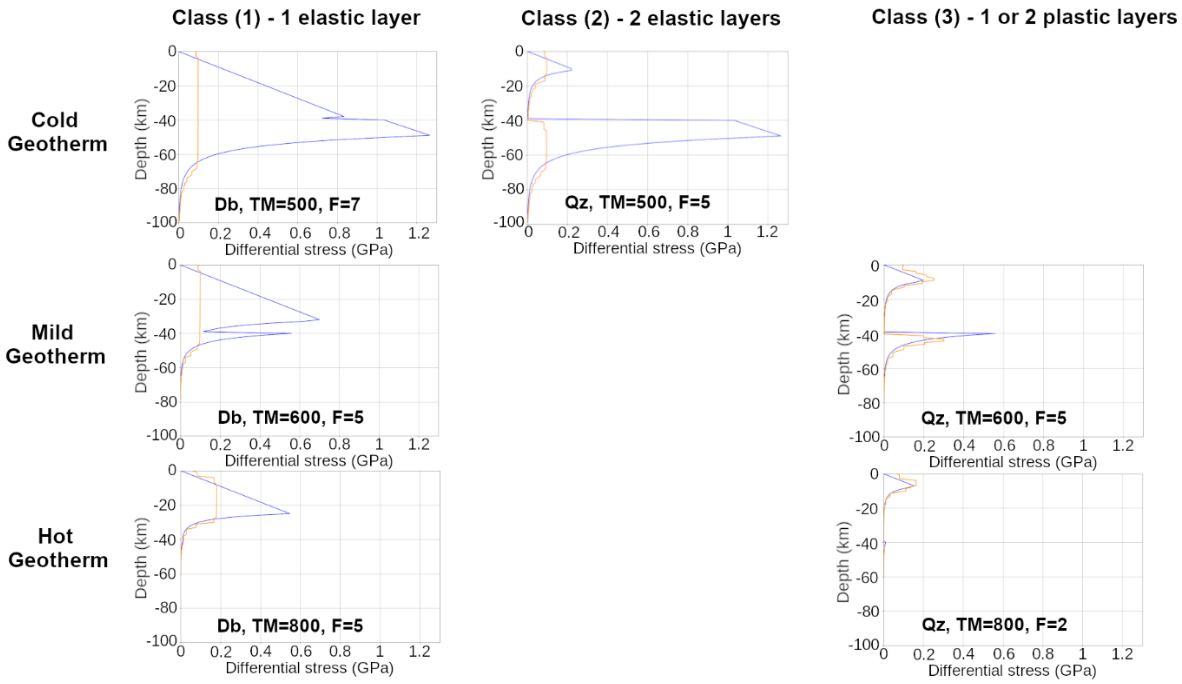

Figure S1. Model differential stress profiles and associated classes. *Blue curves: theoretical brittle / ductile yield stress profiles defined by the geotherm and rheology laws. Orange curves: force-limited differential stress profiles used in our models. For each model, the associated lithosphere integrated resistance is given by F (in 10^{12} N/m). Left, center, and right columns correspond to classes 1, 2, and 3. Top, middle, and bottom rows correspond to cold, mild, and hot geotherms (TM: Moho temperature in ℃). Crust rheology is either quartz (Qz) or diabase (Db).*

(C) MODEL UPLIFT AND STRESS RESPONSE TO EROSION RATES

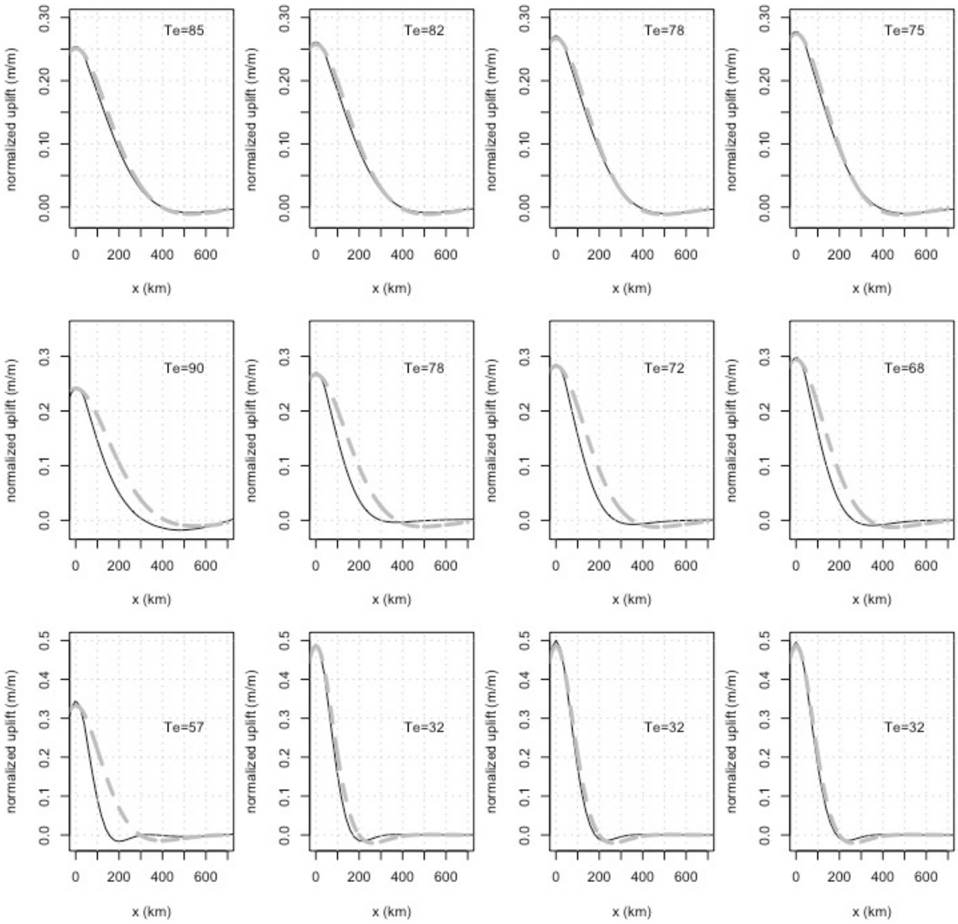

Figure S2. Class 1 uplift at 2 m.y. Uplift is normalized by the amount of erosion after 2 m.y. *Black curves: model uplift at z=3 km. Gray dashed curves: uplift of an elastic plate of thickness T_e (in km). Columns correspond to erosion rates: 4, 40, 100 and 200 m/m.y. Rows correspond to model characteristics: top row - Class 1, cold geotherm, diabase; mid row – Class 1, mild geotherm, diabase; bottom row - Class 1, hot geotherm, diabase.*

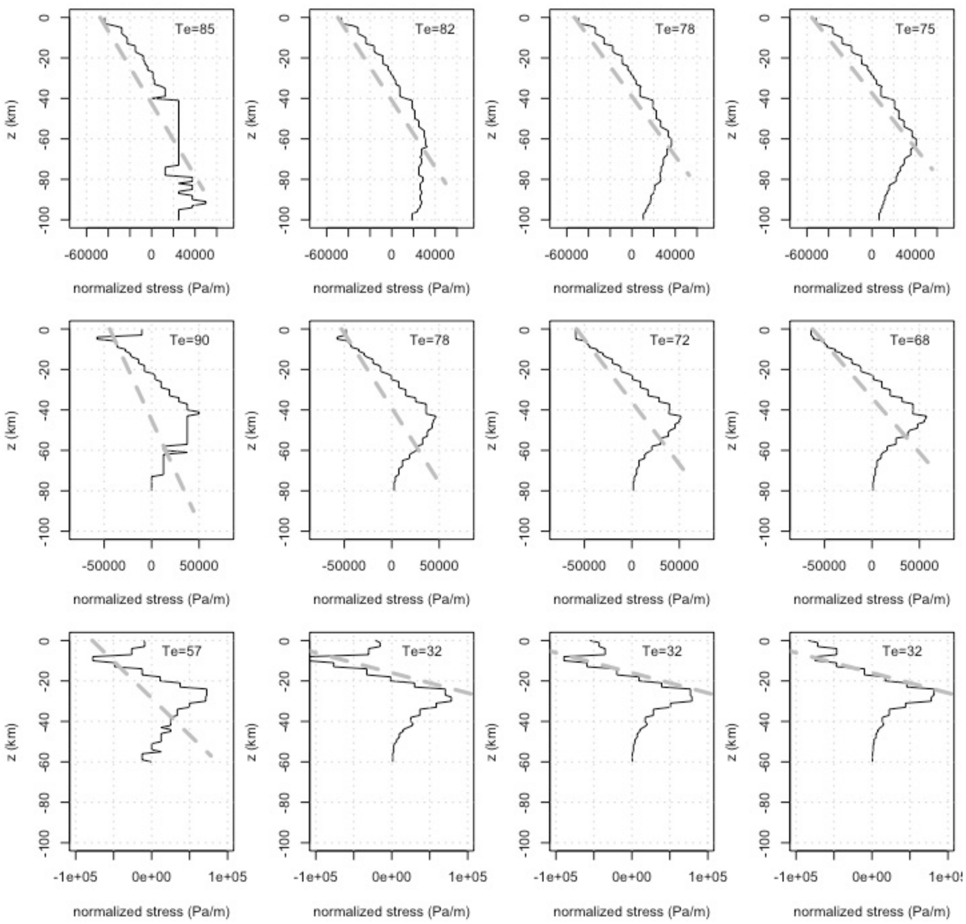

Figure S3. Class (1) horizontal stress at 2 m.y. Stress is normalized by the amount of erosion after 2 m.y.. *Black curves: model stress at the center of erosion x=0 km. Gray dashed curves: bending stress of an elastic plate of thickness T_e (in km). Columns correspond to erosion rates: 4, 40, 100 and 200 m/m.y.. Rows correspond to model characteristics: top row - Class 1, cold geotherm, diabase; mid row – Class 1, mild geotherm, diabase; bottom row - Class 1, hot geotherm, diabase.*

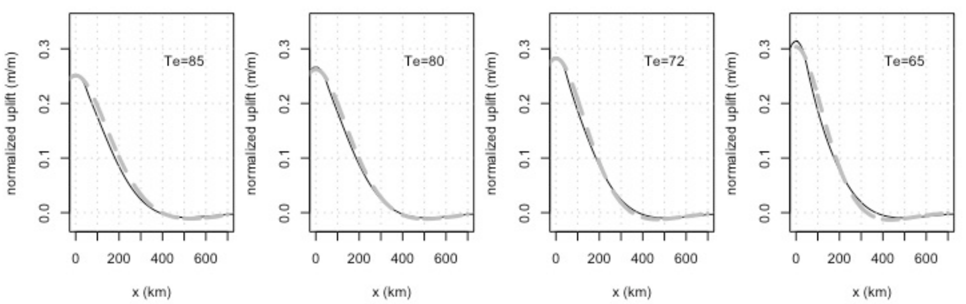

Figure S4. Class (2) uplift at 2 m.y. Uplift is normalized by the amount of erosion after 2 m.y. *Black curves: model uplift at z=3 km. Gray dashed curves: uplift of an elastic plate of* *thickness T_e (in km). Columns correspond to erosion rates: 4, 40, 100 and 200 m/m.y. Model characteristics: Class 2, cold geotherm, quartz.*

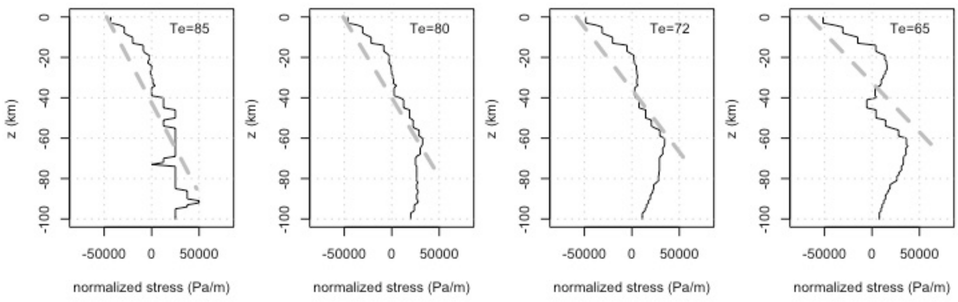

Figure S5. Class 2 horizontal stress at 2 m.y. Stress is normalized by the amount of erosion after 2 m.y. *Black curves: model stress at the center of erosion x=0 km. Gray dashed curves: bending stress of an elastic plate of thickness T_e (in km). Columns correspond to erosion rates: 4, 40, 100 and 200 m/m.y. Model characteristics: Class 2, cold geotherm, quartz.*

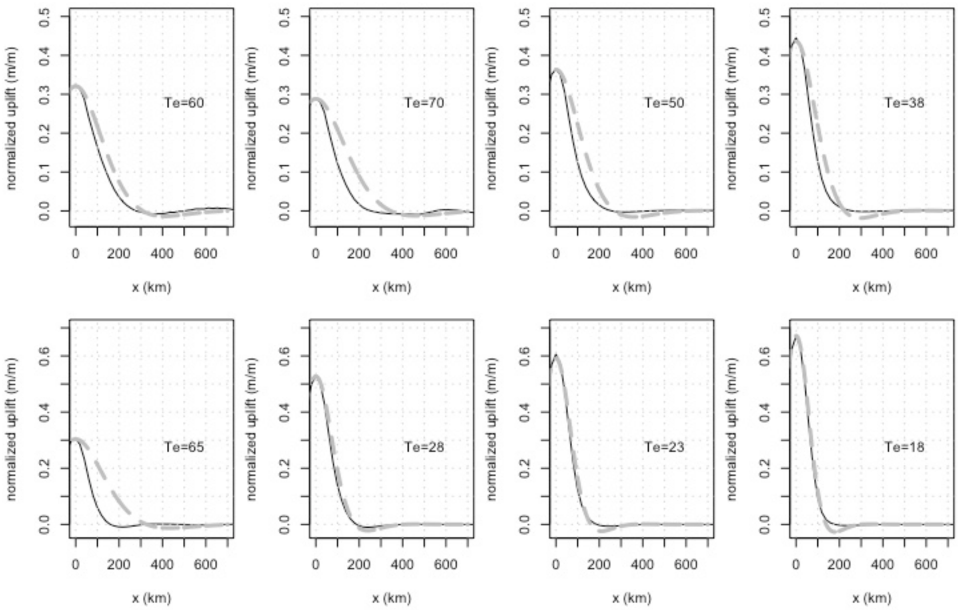

Figure S6. Class 3 uplift at 2 m.y. Uplift is normalized by the amount of erosion after 2 m.y. *Black curves: model uplift at z=3 km. Gray dashed curves: uplift of an elastic plate of thickness T_e (in km). Columns correspond to erosion rates: 4, 40, 100 and 200 m/m.y. Rows correspond to model characteristics: top row - Class 3, mild geotherm, quartz; bottom row - Class 3, hot geotherm, quartz.*

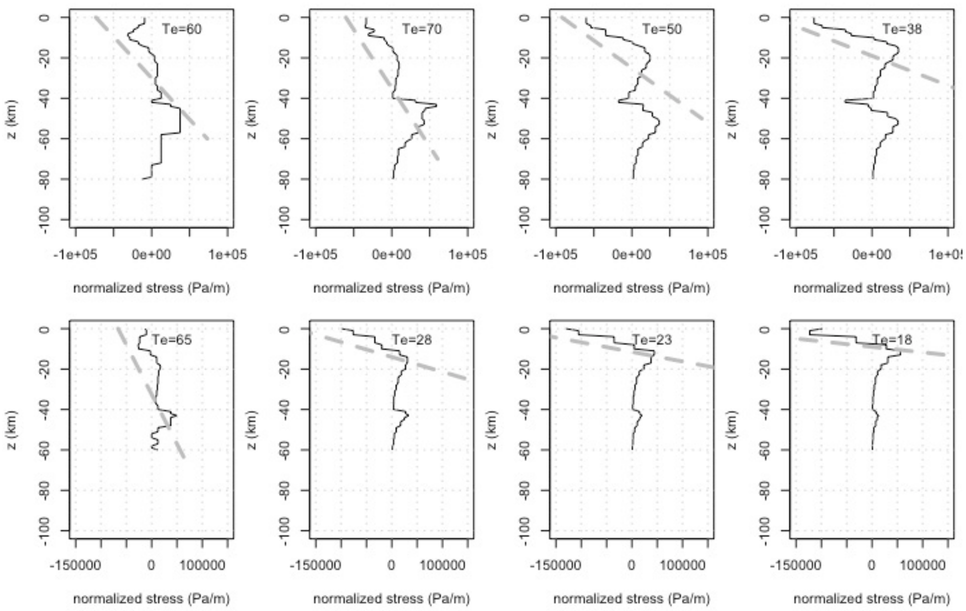

Figure S7. Class 3 horizontal stress at 2 m.y. Stress is normalized by the amount of erosion after 2 m.y. *Black curves: model stress at the center of erosion x=0 km. Gray dashed curves: bending stress of an elastic plate of thickness T_e (in km). Columns correspond to erosion rates: 4, 40, 100 and 200 m/m.y. Rows correspond to model characteristics: top row - Class 3, mild geotherm, quartz; bottom row - Class 3, hot geotherm, quartz.*

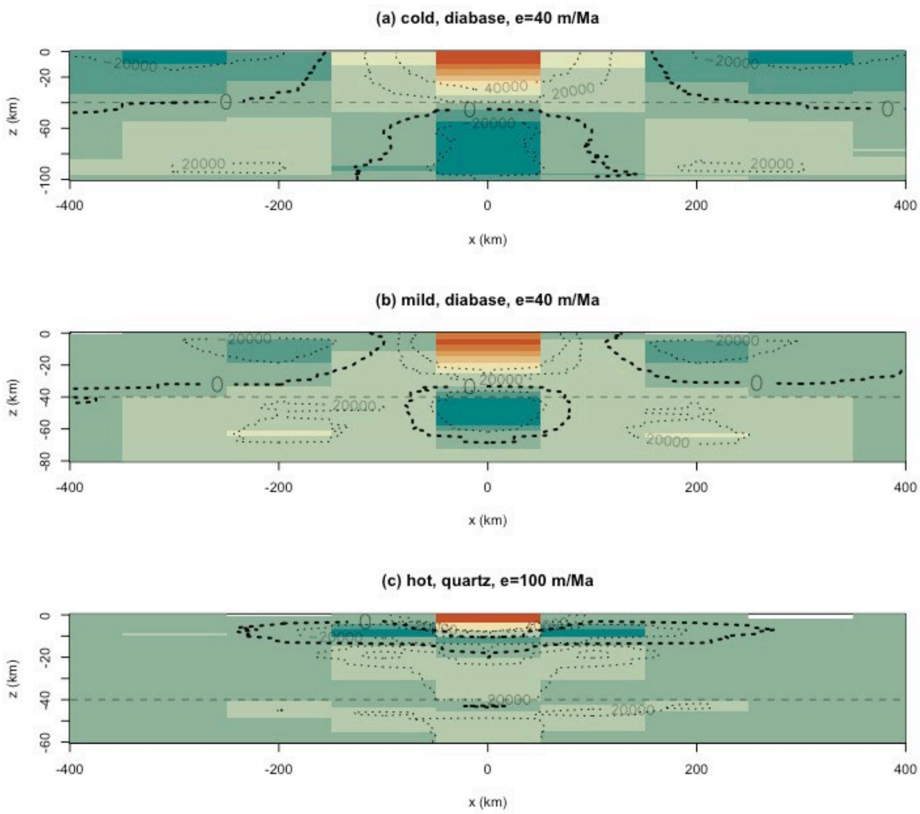

Figure S8. Examples erosion-induced horizontal stress distribution at 2 m.y. for 3 typical models. Stress is normalized by the amount of erosion after 2 m.y. *Dotted lines are 20,000 Pa/m isocontours.*

(C) FAULT STABILITY MARGIN CONSTRUCTION

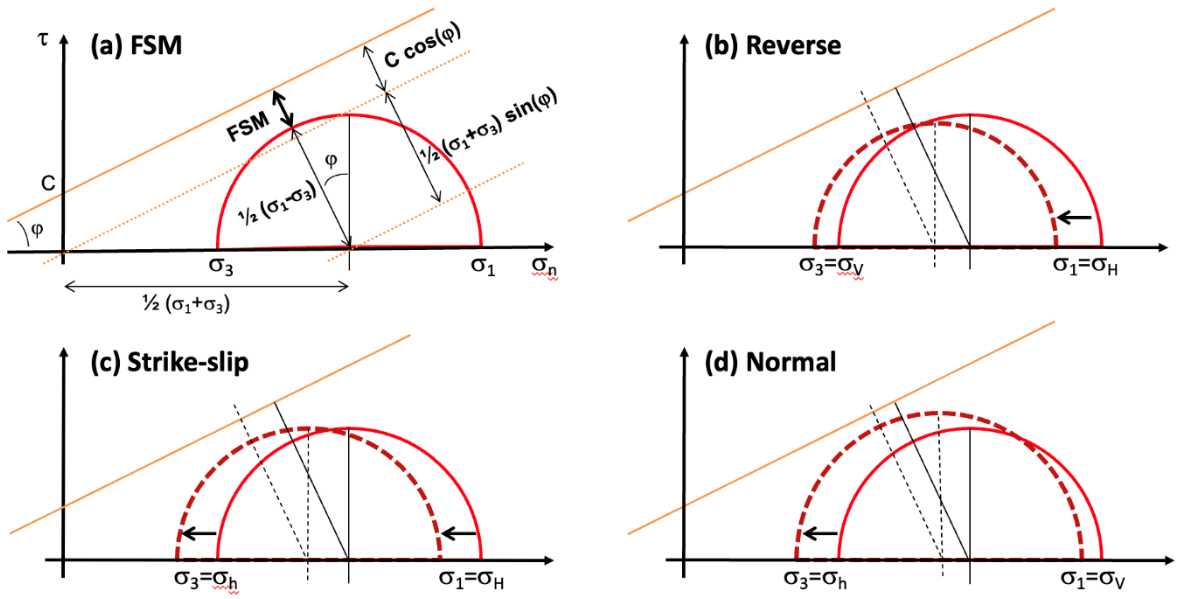

Figure S8. Mohr Circle and Fault Stability Margin (FSM). (a) Geometric construction of FSM calculation relative to Mohr-Coulomb failure criterion (orange line). C and φ: fault cohesion and friction. σ_1 and σ_3: maximum and minimum principal stresses. σ_H, σ_h, and σ_V: maximum horizontal, minimum horizontal, and vertical stresses. (b), (c), and (d) Evolution of Mohr circle due to erosion in isotropic case (cf. text) for reverse, strike-slip, and normal Andersonian fault geometries. Full red circles: original state of stress. Dashed red circles: post-erosion state of stress.

(D) EARTHQUAKE DEPTHS

Table S2: Earthquake rupture extents shown in Figure 3 updated from (Klose and Seeber, 2007)

plate	loc	date	top (km)	bottom (km)	epicenter (km)	M_w	Ref.
AU	Meckering, AU	14/10/1968	0	6	3	6.6	(1)
AU	Lake McKay, AU	24/03/1970	0	8	8	6	(1)

AU	Simpson Desert, AU	28/08/1972	0	8	8	5.6	(1)
AU	Cadoux, AU	02/06/1979	0	6	4	6.1	(1)
AU	Marryat Creek, AU	30/03/1986	0	3	3	5.8	(1)
AU	Tennant 1, AU	22/01/1988	0	6	4.5	6.3	(1)
AU	Tennant 2, AU	22/01/1988	0	7	3	6.4	(1)
AU	Tennant 3, AU	22/01/1988	0	7	4.5	6.6	(1)
NA	Baffin Bay, Canada	04/09/1963	0	7	7	6.1	(1)
NA	Saguenay, Canada	25/11/1988	25	30	29	5.9	(1)
NA	Miramichi, Canada	09/01/1982	3.5	7	7	5.5	(1)
NA	Goodnow, USA	07/10/1983	7	8	7.5	4.8	(1)
NA	Ungava, Canada	25/12/1989	0	5	5	6.0	(1)
NA	Pymatuning, USA	25/09/1998	4	5	4.5	5.3	(1)
NA	Au Sable Forks, USA	20/04/2002	10	13	11.5	5	(1)
IN	Killari, India	29/09/1993	0	6	2.6	6.1	(1)
IN	Bhuj, India	26/01/2001	0	10	26	7.6	(1)
IN	Bhuj, India	26/01/2001	13	30	26	7.6	(1)
AF	Ceres, RSA	29/09/1969	0	6.5	4	6.4	(1)
AF	West Guinea	22/12/1983	0	13	11	6.3	(1)
EU	Schwabian Jura	03/09/1978	3	7.5	6.5	5.0	(1)
EU	North Wales, UK	19/07/1984	20	23	23	5.5	(1)
NA	Mineral, Virginia	23/08/2011	3	8	6	5.8	(2)
AF	Moiyabana, Botswana	03/04/2017	20	30	25	6.5	(3)
AU	Woods Point, AU	22/09/2021	4	13	12	5.9	(4)
NA	Barrow Strait, Canada	08/01/2017	28	35	34	5.9	(5)

Plate: AU – Australia, NA – North America, IN – India, AF – Africa, EU – Europe. loc: earthquake location / name. top and bottom: rupture depth extent. epic.: epicentral depth. Ref.: (1) (Klose and Seeber, 2007), (2) (Horton et al., 2015), (3) (Mulabisana et al., 2021), (4) https://www.src.com.au/largest-earthquake-in-victorias-history/, (5) (Bent et al., 2018).

The earthquake depth histogram in Figure 3 is based on the global SCR earthquake catalogue of (Schulte and Mooney, 2005). Earthquake selection: Year ≥ 1965 (start of global modern network); $M_W \geq 3.5$; total 670 earthquakes.

REFERENCES CITED

Bent, A., Kolaj, M., Ackerley, N., Adams, J., and Halchuk, S., 2018, The 2017 Barrow Strait, Arctic Canada, Earthquake Sequence and Contemporaneous Regional Seismicity: Seismological Research Letters, v. 89, p. 1977–1988, doi:10.1785/0220180100.

Hirth, G., and Kohlstedt, D., 2003, Rheology of the Upper Mantle and Mantle Wedge: a View from the Experimentalists, *in* Inside the Subduction Factory, American Geophysical Union, v. Geophysical Monograph 138, p. 83–105.

Horton, J.W., Shah, A.K., McNamara, D.E., Snyder, S.L., and Carter, A.M., 2015, Aftershocks illuminate the 2011 Mineral, Virginia, earthquake causative fault zone and nearby active faults, *in* The 2011 Mineral, Virginia, Earthquake, and Its Significance for Seismic Hazards in Eastern North America, Geological Society of America, doi:10.1130/2015.2509(14).

Klose, C.D., and Seeber, L., 2007, Shallow Seismicity in Stable Continental Regions: Seismological Research Letters, v. 78, p. 554–562, doi:10.1785/gssrl.78.5.554.

Luan, F.C., and Paterson, M.S., 1992, Preparation and deformation of synthetic aggregates of quartz: Journal of Geophysical Research: Solid Earth, v. 97, p. 301–320, doi:https://doi.org/10.1029/91JB01748.

Mulabisana, T., Meghraoui, M., Midzi, V., Saleh, M., Ntibinyane, O., Kwadiba, T., Manzunzu, B., Seiphemo, O., Pule, T., and Saunders, I., 2021, Seismotectonic analysis of the 2017 moiyabana earthquake (MW 6.5; Botswana), insights from field investigations, aftershock and InSAR studies: Journal of African Earth Sciences, v. 182, p. 104297, doi:10.1016/j.jafrearsci.2021.104297.

Schulte, S.M., and Mooney, W.D., 2005, An updated global earthquake catalogue for stable continental regions: reassessing the correlation with ancient rifts: Geophysical Journal International, v. 161, p. 707–721, doi:10.1111/j.1365-246X.2005.02554.x.

Wilks, K.R., and Carter, N.L., 1990, Rheology of some continental lower crustal rocks: Tectonophysics, v. 182, p. 57–77.